Science Advances
AAAS

advances.sciencemag.org/cgi/content/full/6/45/eabc4882/DC1

Supplementary Materials for

Endogenous DEL-1 restrains melanoma lung metastasis by limiting myeloid cell–associated lung inflammation

Young-Min Hyun, Sang-Uk Seo, Woo Seon Choi, Hyung-Joon Kwon, Dong-Young Kim, Soi Jeong, Gyeong-Yi Kang, Eunbi Yi, Minjung Kim, Hyun Jin Ryu, Mark R. Looney, Eun Young Choi*, Hun Sik Kim*

*Corresponding author. Email: choieun@ulsan.ac.kr (E.Y.C.); hunkim@amc.seoul.kr (H.S.K.)

Published 6 November 2020, *Sci. Adv.* **6**, eabc4882 (2020)
DOI: 10.1126/sciadv.abc4882

The PDF file includes:

Other Supplementary Material for this manuscript includes the following:

(available at advances.sciencemag.org/cgi/content/full/6/45/eabc4882/DC1)

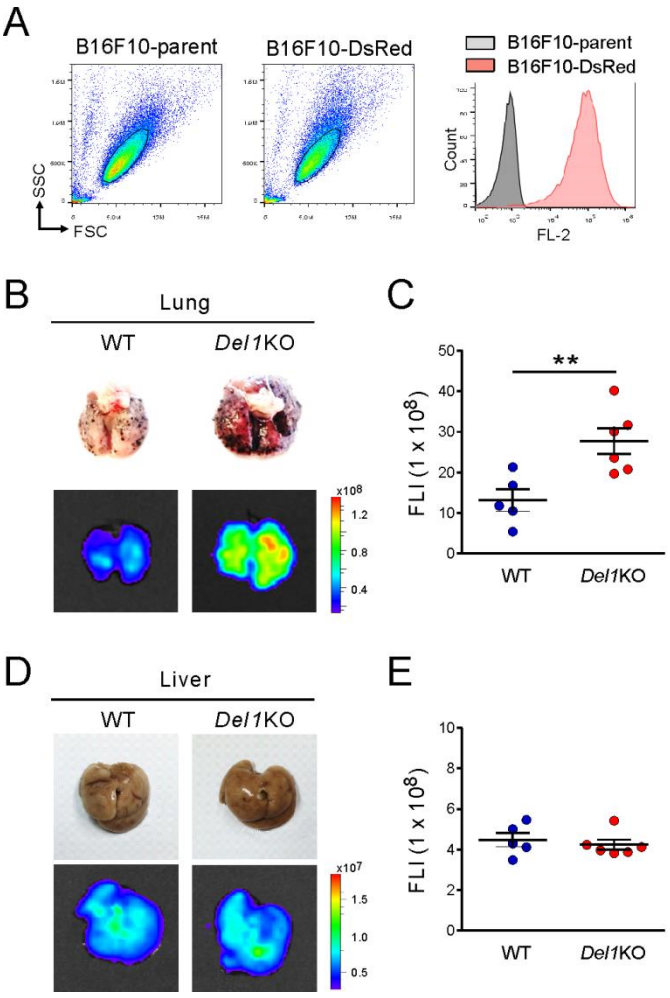

Fig. S1. Melanoma metastasis to the lung but not liver is increased by DEL-1-deficiency. (**A**) Establishment of B16F10 cells expressing DsRed by retroviral transduction. B16F10 cells transduced with retrovirus containing sequence for DsRed were sorted and compared with B16F10 control cells by forward scatter (FSC) and side scatter (SSC) parameters (left) and DsRed expression (right). (**B** and **D**) Representative lung (B) and liver (D) images (top) and the corresponding DsRed fluorescence images (bottom) showing metastases to the lungs and livers of WT (n = 5) or *Del1*KO (n = 6) mice 2 weeks after i.v. injection of 2×10^5 DsRed-tagged B16F10 cells. Photo credit: Hyung-Joon Kwon, University of Ulsan. (**C** and **E**) Quantification of lung and liver metastases by fluorescence intensity (FLI) depicted in (B and D). Data are expressed as mean ± SEM. $^{**}P < 0.01$.

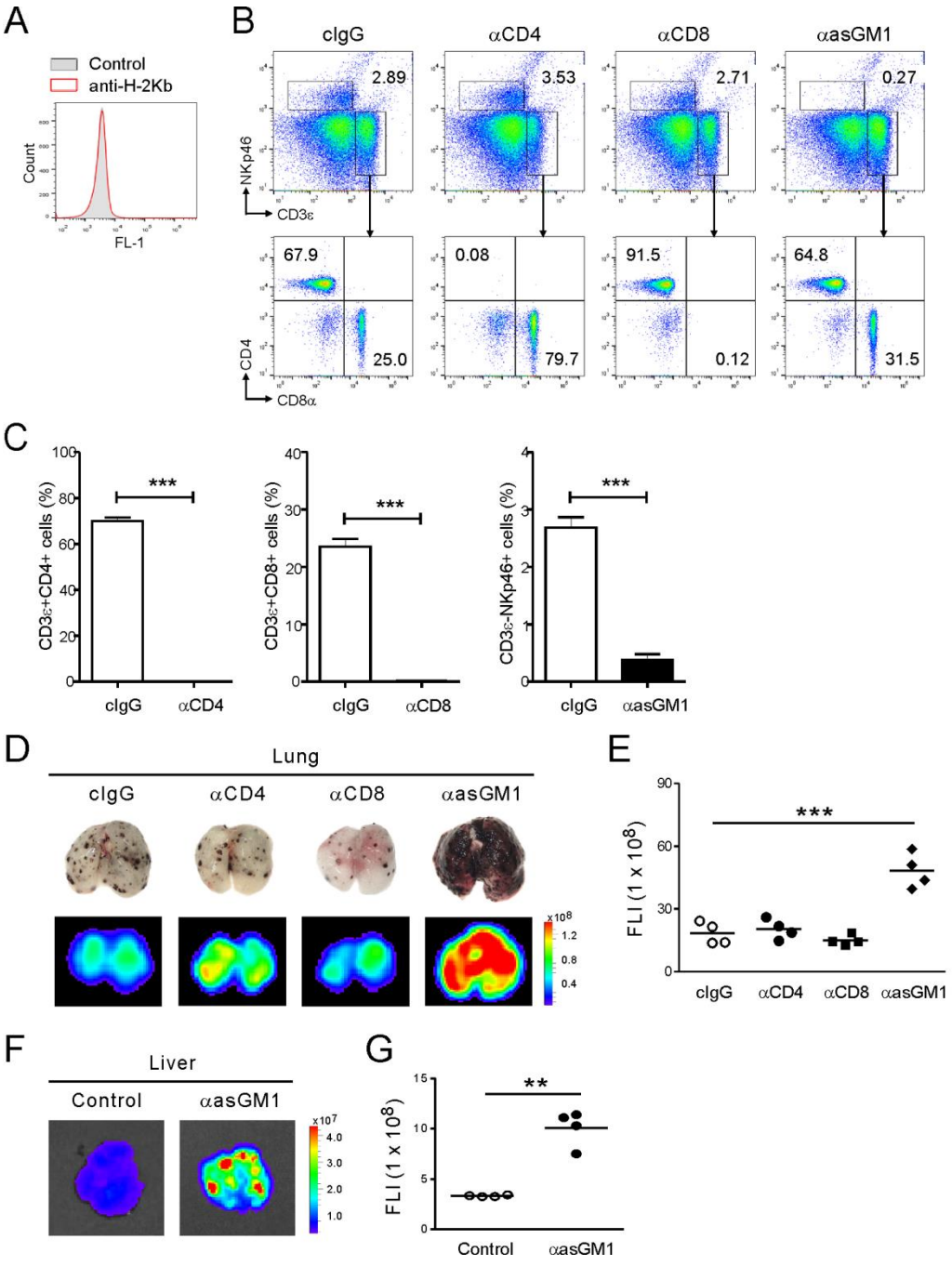

Fig. S2. Pulmonary metastases of B16F10 cells are NK cell-dependent.

(**A**) Representative flow cytometry profile showing the expression of the MHC class-I (H-2Kb) on DsRed-B16F10 cells (red solid line). Isotype control staining is shown as a shaded histogram. (**B** to **G**) C57BL/6 mice (*n* = 4 per group) were treated with i.p. injection of control IgG (150 μg), anti-CD4 (150 μg), anti-CD8 (150 μg), or anti-asialo-GM1 (10 μL) before an i.v. injection of 2 × 10^5 B16F10 cells expressing DsRed and twice a week treatment thereafter. After 14 days later,

mice were euthanized and the frequencies of CD4 T cells ($CD3\varepsilon^+CD4^+$), CD8 T cells ($CD3\varepsilon^+CD8^+$), or NK cells ($CD3\varepsilon^-NKp46^+$) in the spleen of each group are shown as representative flow cytometric profile (B) and graph (C). (**D)** Representative lung images (top) and the corresponding DsRed fluorescence images (bottom) showing the increased metastases to the lungs of mice treated with anti-asialo-GM1. Photo credit: Woo Seon Choi, University of Ulsan. (**E**) Quantification of lung metastases by fluorescence intensity (FLI) depicted in (D). (**F**) Representative liver images (top) and the corresponding DsRed fluorescence images (bottom) showing the increased liver metastases after anti-asialo-GM1 treatment. (**G**) Quantification of liver metastases by FLI depicted in (F). Data are expressed as mean ± SD (C). Horizontal bars indicate the means (E, G). $^{**}P < 0.01$; $^{***}P < 0.001$.

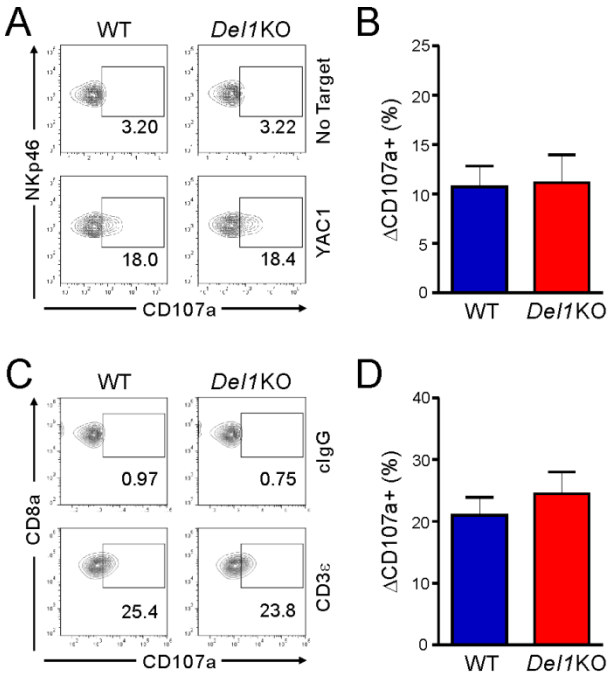

Fig. S3. DEL-1 is dispensable for cytotoxic potential of NK cells and T cells.
(**A** and **B**) Splenic NK cells were isolated from WT and *Del1*KO mice (n = 6, each group) and incubated with YAC1 target cells in a 1:1 ratio for 4 h. Cytotoxic degranulation was measured by determining surface expression of CD107a on $CD3\varepsilon^{-}NKp46^{+}$ NK cells. Representative result (A) and graph (B) showing percent increase of $CD107a^{+}$ NK cells after stimulation with YAC1 cells relative to $CD107a^{+}$ NK cells without stimulation ($\Delta CD107a^{+}$ cells). (**C** and **D**) Splenic $CD8^{+}$ T cells were isolated from WT and *Del1*KO mice (n = 5, each group) and cocultured with P815 target cells preincubated with either isotype control antibody (cIgG) or anti-CD3ε antibody in a 1:1 ratio for 4 h. Cytotoxic degranulation was measured by surface expression of CD107a on $CD3\varepsilon^{+}CD8a^{+}$ T cells. Representative result (C) and graph (D) showing percent increase of $CD107a^{+}$ $CD8^{+}$ T cells after stimulation with anti-CD3ε-coated P815 cells relative to those without stimulation ($\Delta CD107a^{+}$ cells). Data are expressed as mean ± SD.

A

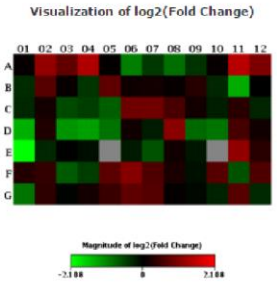

Layout	01	02	03	04	05	06	07	08	09	10	11	12
A	Ackr3 **1.03** OKAY	Aicda **2.27** B	Bcl2 **1.71** OKAY	Bcl2l1 **2.64** OKAY	Ccl2 **1.02** OKAY	Ccl20 **-2.04** OKAY	Ccl22 **-1.38** OKAY	Ccl28 **-1.85** B	Ccl4 **-1.34** OKAY	Ccl5 **1.05** OKAY	Ccr1 **2.82** OKAY	Ccr10 **2.00** OKAY
B	Ccr2 **-1.27** OKAY	Ccr4 **1.62** OKAY	Ccr5 **1.05** OKAY	Ccr7 **-1.34** OKAY	Ccr9 **1.70** OKAY	Cd274 **1.09** OKAY	Csf1 **1.11** OKAY	Csf2 **1.04** OKAY	Csf3 **1.22** B	Ctla4 **-1.25** OKAY	Cxcl1 **-2.61** A	Cxcl10 **-1.01** OKAY
C	Cxcl11 **-1.25** A	Cxcl12 **1.12** OKAY	Cxcl2 **-1.51** OKAY	Cxcl5 **-1.42** OKAY	Cxcl9 **-1.70** OKAY	Cxcr1 **1.87** OKAY	Cxcr2 **1.87** OKAY	Cxcr3 **1.50** OKAY	Cxcr4 **1.11** OKAY	Cxcr5 **-1.18** OKAY	Egf **1.26** OKAY	Egfr **-1.23** OKAY
D	Fasl **-2.68** OKAY	Foxp3 **1.19** OKAY	Gbp2b **-2.31** OKAY	Gzma **-2.44** OKAY	Gzmb **-1.90** OKAY	H2-D1 **1.09** OKAY	H2-K1 **-1.17** OKAY	Hif1a **2.17** OKAY	Ido1 **-1.79** OKAY	Ifng **-1.91** OKAY	Igf1 **1.48** OKAY	Il10 **1.10** B
E	Il12a **-4.31** A	Il12b **-1.25** OKAY	Il13 **-1.02** OKAY	Il15 **-1.08** OKAY	Il17a **1.23** C	Il1a **-1.16** OKAY	Il1b **-1.50** OKAY	Il1r1 **1.09** OKAY	Il2 **-1.14** B	Il22 **1.23** C	Il23a **2.27** OKAY	Il4 **1.24** OKAY
F	Il5 **1.21** OKAY	Il6 **1.34** OKAY	Irf1 **-1.66** OKAY	Kitl **-1.41** OKAY	Mif **1.68** OKAY	Myc **2.14** OKAY	Myd88 **1.55** OKAY	Nfkb1 **1.16** OKAY	Nos2 **-1.10** OKAY	Pdcd1 **1.63** OKAY	Ptgs2 **-1.59** OKAY	Spp1 **1.55** OKAY
G	Stat1 **-1.90** OKAY	Stat3 **1.29** OKAY	Tgfb1 **-1.02** OKAY	Tlr2 **1.12** OKAY	Tlr3 **1.38** OKAY	Tlr4 **1.70** OKAY	Tlr7 **1.60** OKAY	Tlr9 **1.04** OKAY	Tnf **-1.04** OKAY	Tnfsf10 **-1.22** OKAY	Trp53 **1.63** OKAY	Vegfa **-1.26** OKAY

B

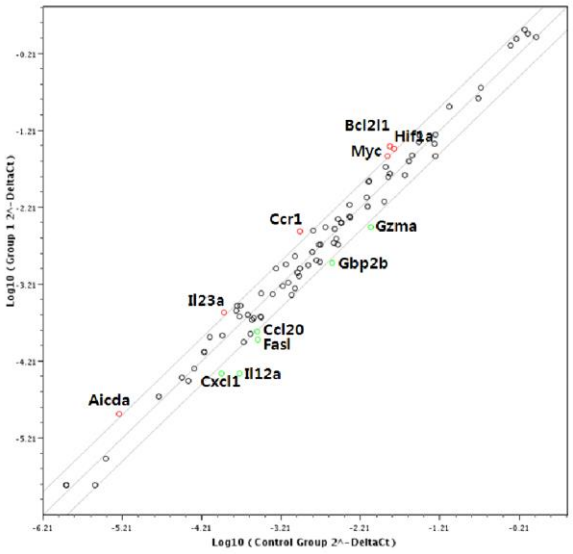

Fig. S4. Association of DEL-1 deficiency with gene expression profiles related to inflammation and impaired immune surveillance.

(**A**) Effect of DEL-1 deficiency on the expression of genes central to cancer inflammation and immunity crosstalk in the metastasis-bearing lungs. Representative Cancer Inflammation and Immunity Crosstalk RT^2 profiler PCR array result showing fold changes between the *Del1*KO and control WT mouse group by means of a heat map (top) and gene tables (bottom). (**B**) Representative scatter plot. Fold changes > 2 were considered to represent significant gene dysregulation through either upregulation (red) or downregulation (green).

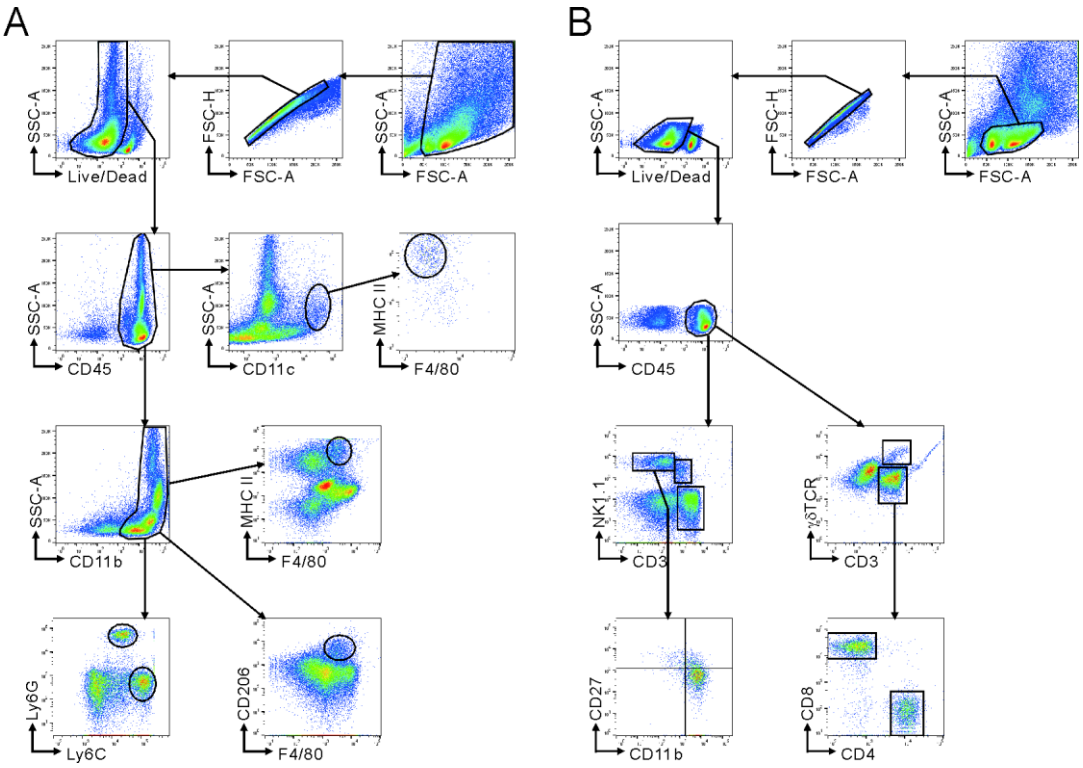

Fig. S5. Flow cytometric gating strategy.

Profiles showing the gating strategy for identifying different myeloid cells and lymphocytes in the metastasis-bearing lungs of this study. (**A**) Gating strategy for myeloid panel: FSC vs. SSC, FSC-Area vs. FSC-Height, Live/Dead vs. SSC, CD45 vs. SSC, then CD11c vs. SSC and F4/80 vs. MHC II, or CD11b vs. SSC, F4/80 vs. MHC II, Ly6C vs. Ly6G, and F4/80 vs. CD206. (**B**) Gating strategy for lymphocyte panel: FSC vs. SSC, FSC-Area vs. FSC-Height, Live/Dead vs. SSC, CD45 vs. SSC, then CD3 vs. NK1.1 and CD11b vs. CD27, or CD3 vs. γδTCR and CD4 vs. CD8.

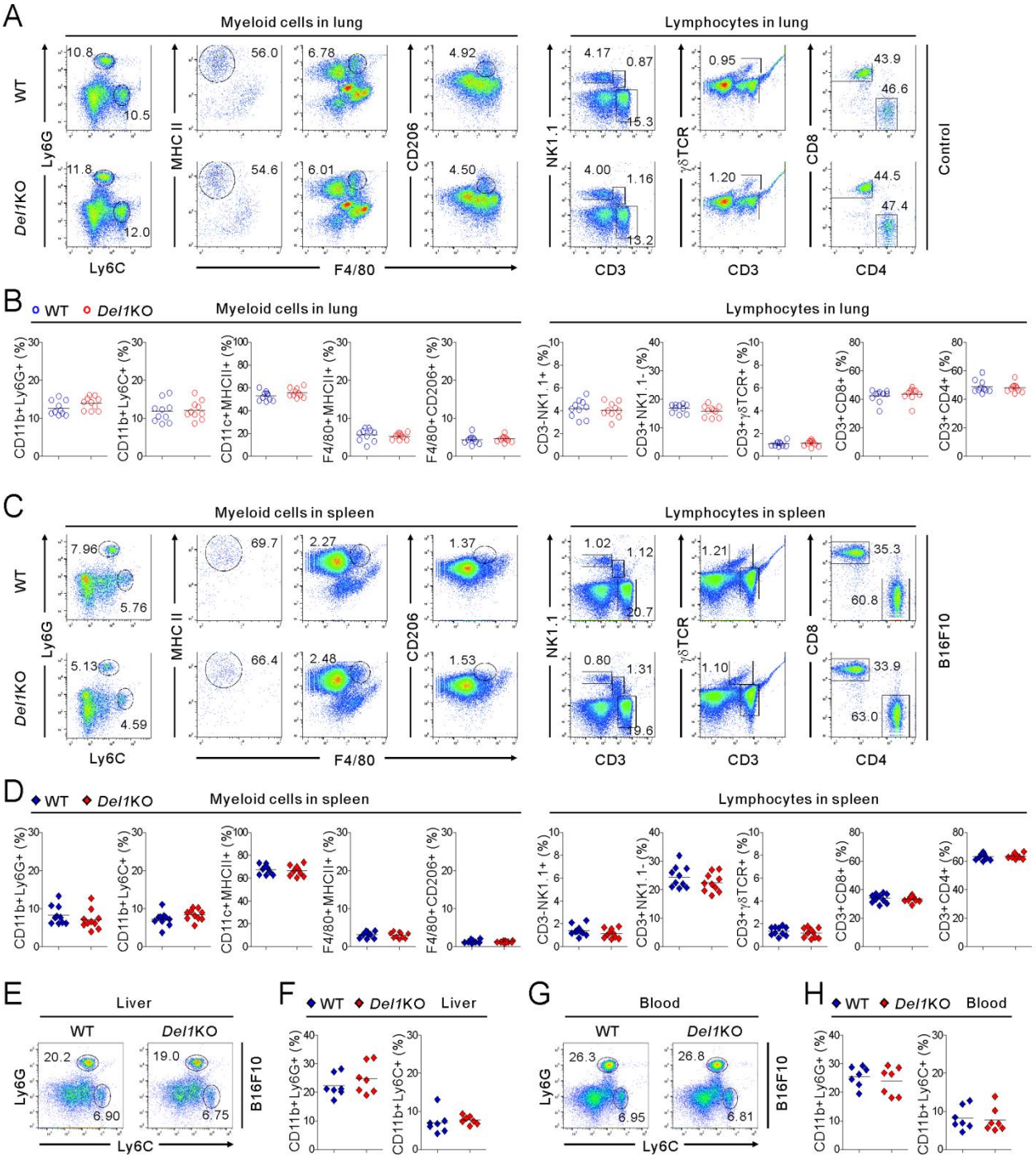

Fig. S6. DEL-1 deficiency does not affect immune cell presence in the lung of control tumor-free mice or in the spleen of mice with pulmonary metastasis.

(**A** and **B**) Representative (A) and quantitative (B) flow cytometric analysis of different myeloid cells ($CD11b^+Ly6G^+$ neutrophils, $CD11b^+Ly6C^+$, monocytes, $CD11c^+MHCII^+$ dendritic cells, and $F4/80^+MHCII^+$ M1-like and $F4/80^+CD206^+$ M2-like macrophages) and lymphocytes ($CD3^-$

NK1.1$^+$ NK cells, CD3$^+$γδ T cells, CD8$^+$ T cells, and CD4$^+$ T cells) among CD45$^+$ cell populations in the lungs of control tumor-free WT and *Del1*KO mice (*n* = 10, each group). (**C** and **D**) Representative (C) and quantitative (D) flow cytometric analysis of different myeloid cells and lymphocytes among CD45$^+$ cell populations in the spleens of WT and *Del1*KO mice (*n* = 10, each group) on day 14 after i.v. injection of B16F10 cells. (**E** to **H**) Representative (E and G) and quantitative (F and H) flow cytometric analysis of different myeloid cells, graphed on Ly6C by Ly6G dot plots, among CD45$^+$ cell populations in the livers (E and F) and peripheral blood (G and H) of WT and *Del1*KO mice (*n* = 7, each group) on day 14 after i.v. injection of B16F10 cells. Horizontal bars indicate the means.

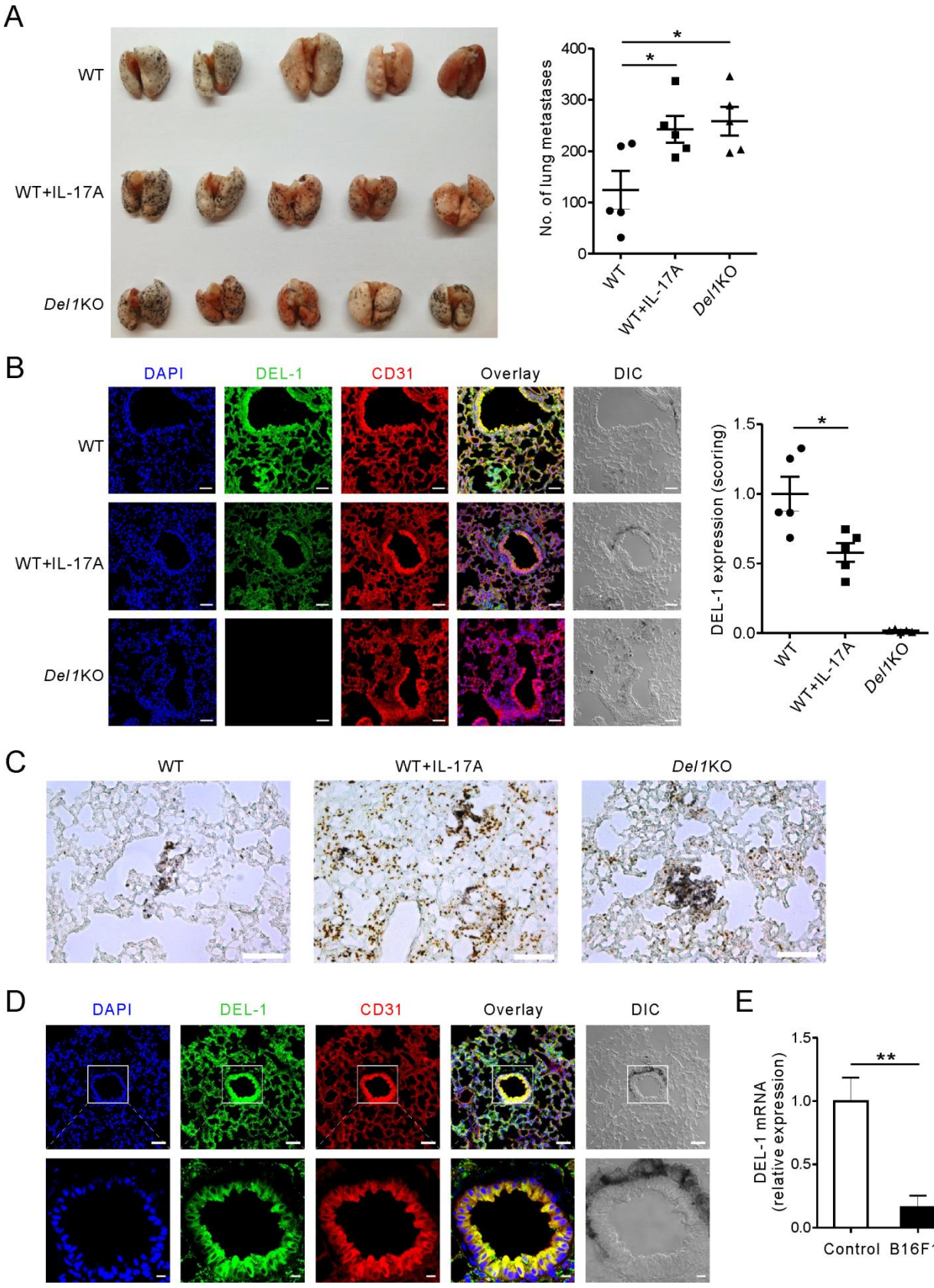
A
WT
WT+IL-17A
Del1KO
No. of lung metastases
400
300
200
100
0
*
*
WT
WT+IL-17A
Del1KO
B
DAPI
DEL-1
CD31
Overlay
DIC
WT
WT+IL-17A
Del1KO
DEL-1 expression (scoring)
1.5
1.0
0.5
0.0
*
WT
WT+IL-17A
Del1KO
C
WT
WT+IL-17A
Del1KO
D
DAPI
DEL-1
CD31
Overlay
DIC
E
DEL-1 mRNA (relative expression)
1.5
1.0
0.5
0.0
**
Control
B16F10

Fig. S7. IL-17A increases melanoma lung metastasis linked to neutrophil accumulation and reduced DEL-1 expression.

(**A**) Macroscopic images of the lungs showing metastatic nodules in WT and *Del1*KO mice (n = 5 per group) i.v. injected with B16F10 cells (5×10^5 cells/mouse on day 0), and those in a separate group of WT mice that was additionally administered with murine IL-17A (intranasal injection; 250 ng/dose on days 1, 3 and 5). Lung tissues were collected on day 7. Quantification of lung metastases (numbers of black nodules on the surface of lungs) is shown in the right panel. Photo credit: Dong-Young Kim, University of Ulsan. (**B**) Representative lung sections showing endothelial DEL-1 expression in mice depicted in (A). Green, DEL-1; red, CD31; blue, DAPI. The corresponding DIC images are shown to indicate lung metastatic melanoma. Scale bar = 50 μm. Quantification of DEL-1 expression is shown in the right panel. (**C**) Representative lung sections showing neutrophil infiltration in mice depicted in (A). Brown, neutrophils (labeled with Ly6G); black, B16F10 cells. Scale bar = 100 μm. (**D**) Representative lung sections showing endothelial DEL-1 expression in metastasis-bearing lung of WT mice. Green, DEL-1; red, CD31; blue, DAPI. Metastatic melanoma is shown by the corresponding DIC image. Magnified images (bottom panel) show peritumoral loss of DEL-1 and CD31 expression. Scale bar = 50 μm (top) and 20 μm (bottom). (**E**) Relative expression of DEL-1 in metastatic lung tissues as assessed by qRT-PCR. WT mice (n = 4 per group) were injected with 5×10^5 B16F10 cells via tail vein. Lung tissues were collected on day 7. Levels of 18S were used for normalization, and the expression of DEL-1 in tumor-free control lung was set to 1.0. Data are expressed as mean ± SEM. *$P < 0.05$.

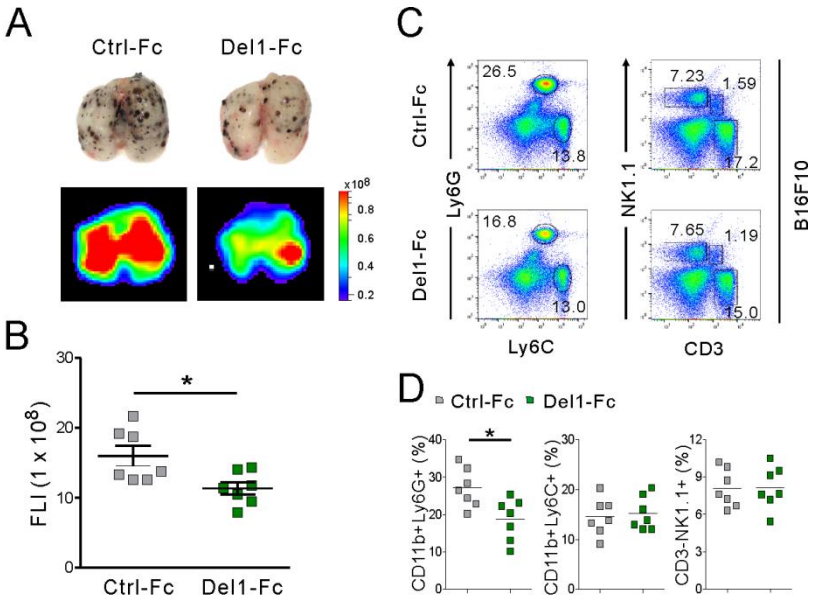

Fig. S8. Del-1-Fc administration after tumor inoculation alleviates melanoma lung metastasis and neutrophil accumulation.

(**A** and **B**) C57BL/6 mice were i.v. inoculated with 2×10^5 DsRed-tagged B16F10 cells. Mice were then i.v. administered with control-Fc or Del-1-Fc 2 h after tumor inoculation and twice per week treatment thereafter. (A) Representative lung images (top) and the corresponding DsRed fluorescence images (bottom) demonstrating lung metastases (n = 7 per group) on day 14 after tumor implantation. Photo credit: Woo Seon Choi, University of Ulsan. (B) Quantification of lung metastases by FLI depicted in (A). (**C** and **D**) Representative (C) and quantitative (D) flow cytometric analysis of different myeloid cells and lymphocytes, graphed on Ly6C by Ly6G and CD3 by NK1.1 dot plots, respectively, in the metastasis-bearing lungs depicted in (A). Data are expressed as mean ± SEM (B). Horizontal bars indicate the means (D). *P < 0.05.

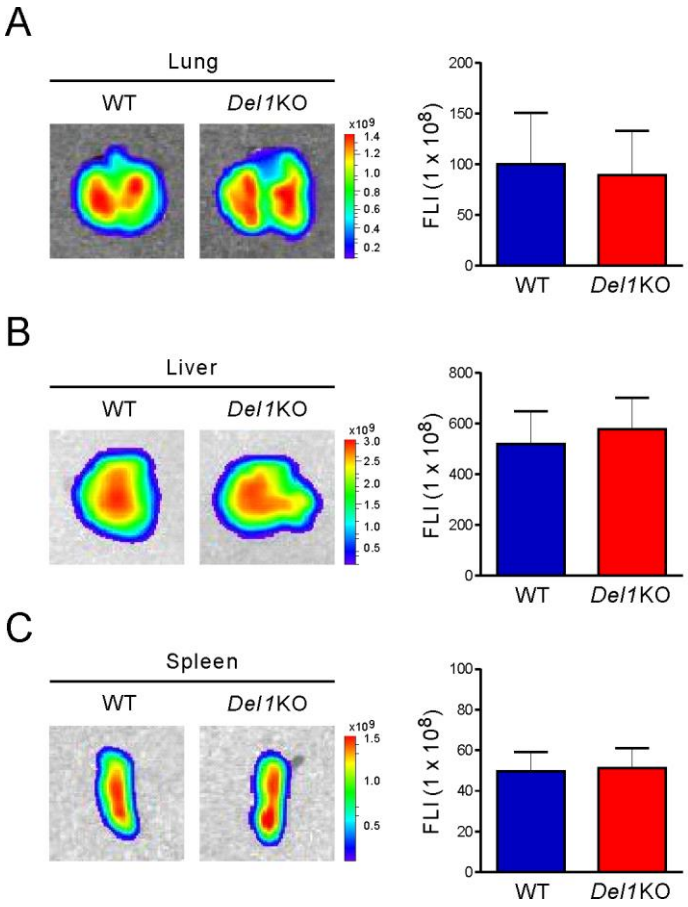

Fig. S9. DEL-1 deficiency does not affect initial seeding of B16F10 cells in the lung.
WT (*n* = 5) or *Del1*KO (*n* = 6) mice were i.v. injected with XenoLight DiR fluorescent dye-stained B16F10 cells and were euthanized at different time points for the measurement of FLI. Representative fluorescence imaging of lungs (**A**), livers (**B**), and spleens (**C**) at 2 h post-challenge of labeled B16F10 cells. Fluorescence-based quantification of XenoLight DiR dye-positive cells detected in the indicated organs is shown on the right panel. Data are expressed as mean ± SD.

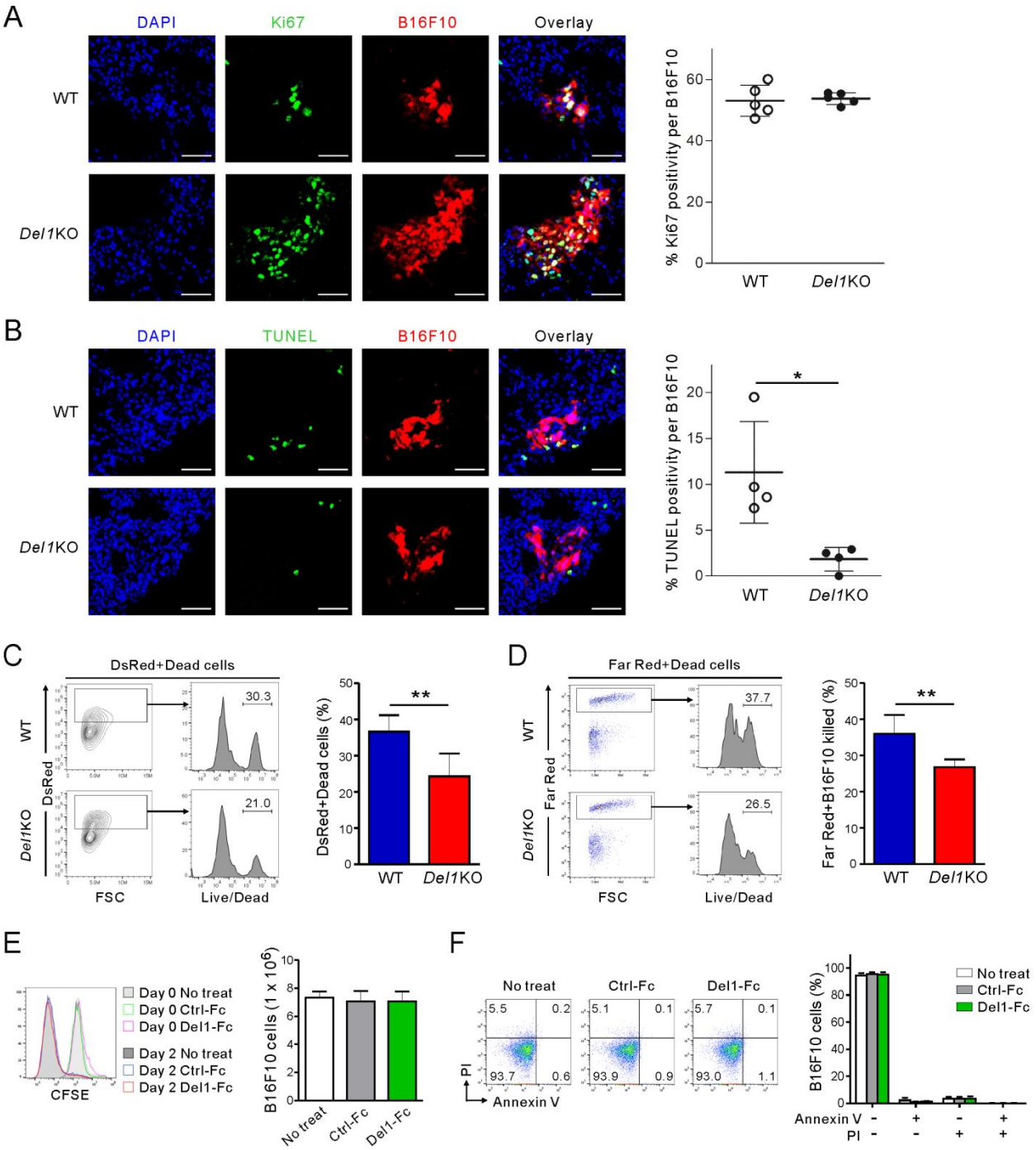

Fig. S10. Attenuated NK cell-mediated clearance of B16F10 cells in the metastasis-bearing lung of *Del1*KO mice.

(**A**) Representative lung sections showing *in situ* proliferation of DsRed-B16F10 cells in metastasis-bearing lung of WT and *Del1*KO mice (n = 5, each group) on day 7 of tumor implantation. Green, Ki67; red, B16F10; blue, DAPI. Scale bars = 50 μm. Quantification of proliferating B16F10 cells is shown in the right panel. (**B**) Representative lung sections showing

in situ apoptosis of DsRed-B16F10 cells in mice (n = 4, each group) depicted in (A). Green, TUNEL; red, B16F10; blue, DAPI. Scale bars = 50 μm. Quantification of TUNEL-positive B16F10 cells is shown in the right panel. (**C**) Representative flow cytometric analysis of dead DsRed-B16F10 cells in the metastasis-bearing lungs of WT and *Del1*KO mice (n = 4, each group) after 14 day of tumor implantation. Cell death was measured after staining of lung single cells with Live/Dead fixable green dead cell dye. Quantification of Live/Dead stain-positive dead cells among DsRed-B16F10 cells is shown in the right panel. (**D**) Representative flow cytometric analysis of NK cell cytotoxicity in the metastasis-bearing lungs of WT and *Del1*KO mice (n = 4, each group) depicted in (C). Cytotoxicity was measured after *in vitro* co-culture with Far Red-labeled B16F10 cells for 6 h, followed by staining with Live/Dead Green dead cell dye. Quantification of Live/Dead stain-positive dead cells of total Far Red-labeled B16F10 cells is shown in the right panel. (**E**) Representative flow cytometric analysis of CFSE-labeled B16F10 cells following treatment with control-Fc or Del-1-Fc for 48 h (n = 4, each group). Quantification of B16F10 cells after the treatment is shown in the right panel. (**F**) Representative flow cytometric analysis of B16F10 cell viability following treatment with control-Fc or Del-1-Fc for 3 days (n = 4, each group). Cell viability was assessed by Annexin V-FITC and PI staining and quantified in the right panel. Data are expressed as mean ± SEM. (A, B) and mean ± SD (C, D, E, F).*P < 0.05; **P < 0.01.

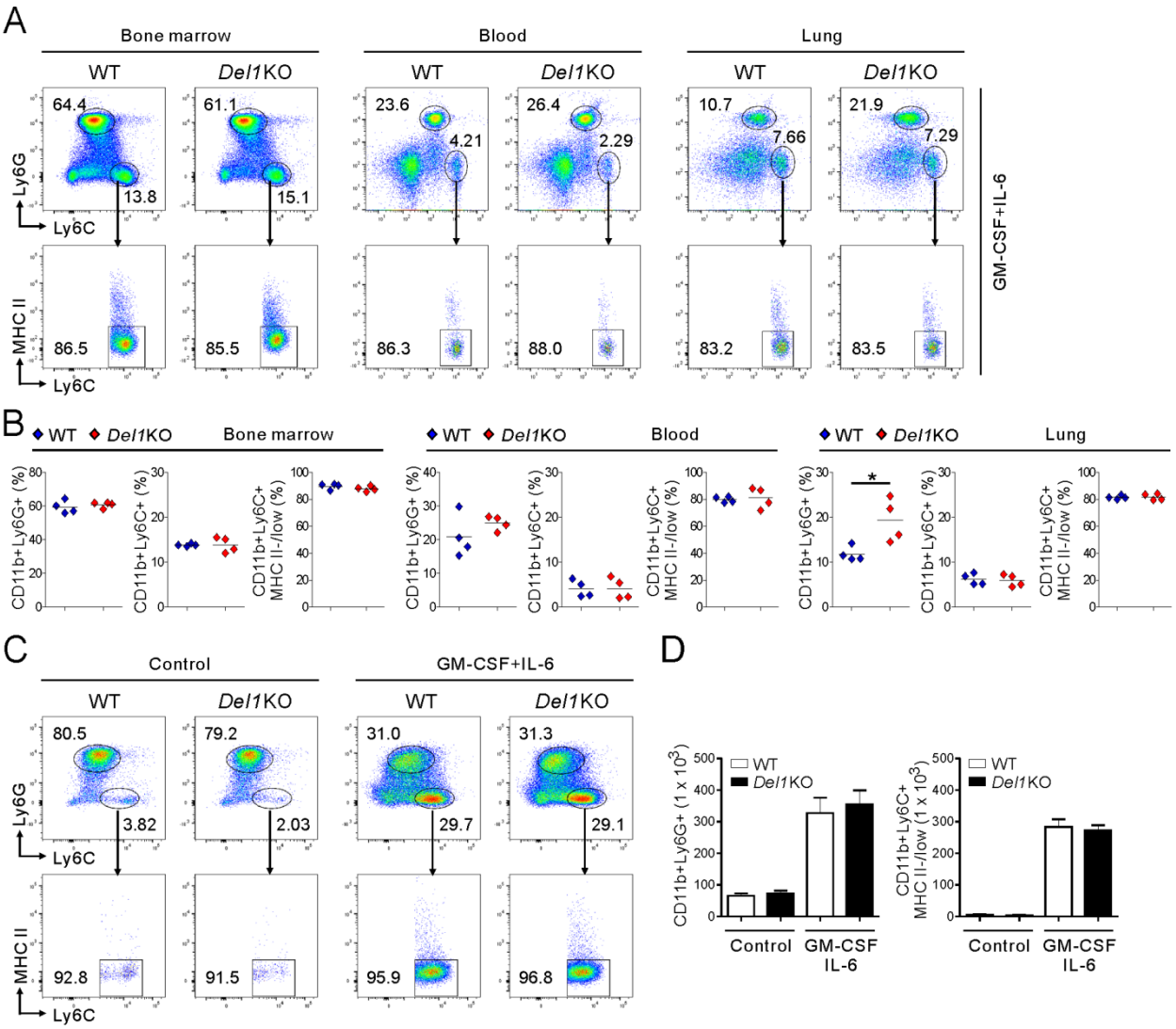

Fig. S11. DEL-1 deficiency enhances neutrophil accumulation in the lung upon GM-CSF and IL-6 treatment.

(**A** and **B**) Effect of *in vivo* GM-CSF and IL-6 treatment on neutrophil mobilization of WT and *Del1*KO mice (n = 4 per group). Representative (A) and quantitative (B) flow cytometric analysis of $CD11b^{+}Ly6G^{+}$ neutrophils and $CD11b^{+}Ly6C^{+}MHC\ II^{-/low}$ monocytes among $CD45^{+}$ cell populations in the BM, blood, and lung of WT and *Del1*KO mice i.p. administered with GM-CSF and IL-6 for 3 consecutive days. (**C** and **D**) *In vitro* myelopoiesis assay of WT and *Del1*KO BM cells upon treatment with GM-CSF and IL-6 for 4 days (n = 5, each group of independent BM isolations). Representative (C) and quantitative (D) flow cytometric analysis of $CD11b^{+}Ly6G^{+}$ neutrophils and $CD11b^{+}Ly6C^{+}MHC\ II^{-/low}$ monocytes among $CD45^{+}$ cell populations after the stimulation. Data are expressed as mean ± SD (D). Horizontal bars indicate the means (B). *$P < 0.05$.

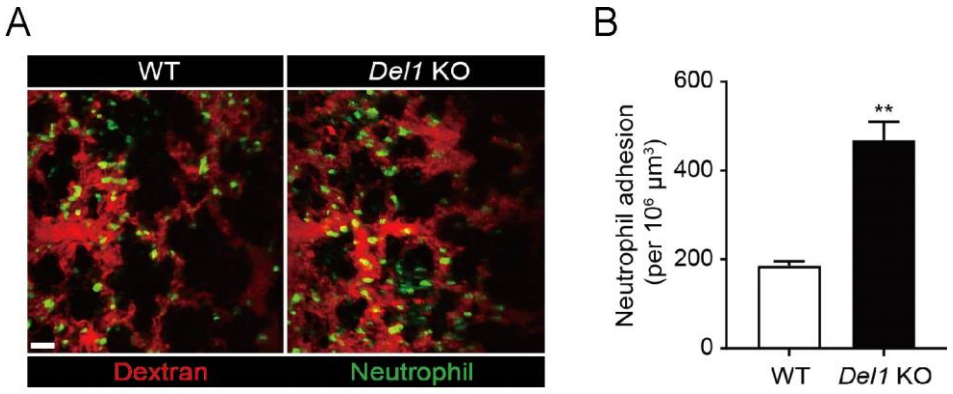

Fig. S12. DEL-1 deficiency enhances neutrophil adhesion to the luminal side of blood vessels.

(**A**) Two-photon intravital imaging of the lungs of LysM-GFP/WT or LysM-GFP/*Del1* KO mice was conducted after 5 days post-i.v. injection of DsRed-B16F10 cells. Texas Red-dextran was i.v. injected to visualize blood flow. Imaging was performed for 20 min, and representative snapshots were presented (n = 3, each group). Scale bar, 50 μm. (**B**) Neutrophils adhered to the luminal side of blood vessels were counted from the intravital imaging of the lungs of LysM-GFP/WT or LysM-GFP/*Del1* KO mice. (n = 3, each group). The number of adherent neutrophils was measured per volume of the blood vessel (10^6 μm^3). Data are expressed as mean ± SEM. $^{**}P < 0.01$.

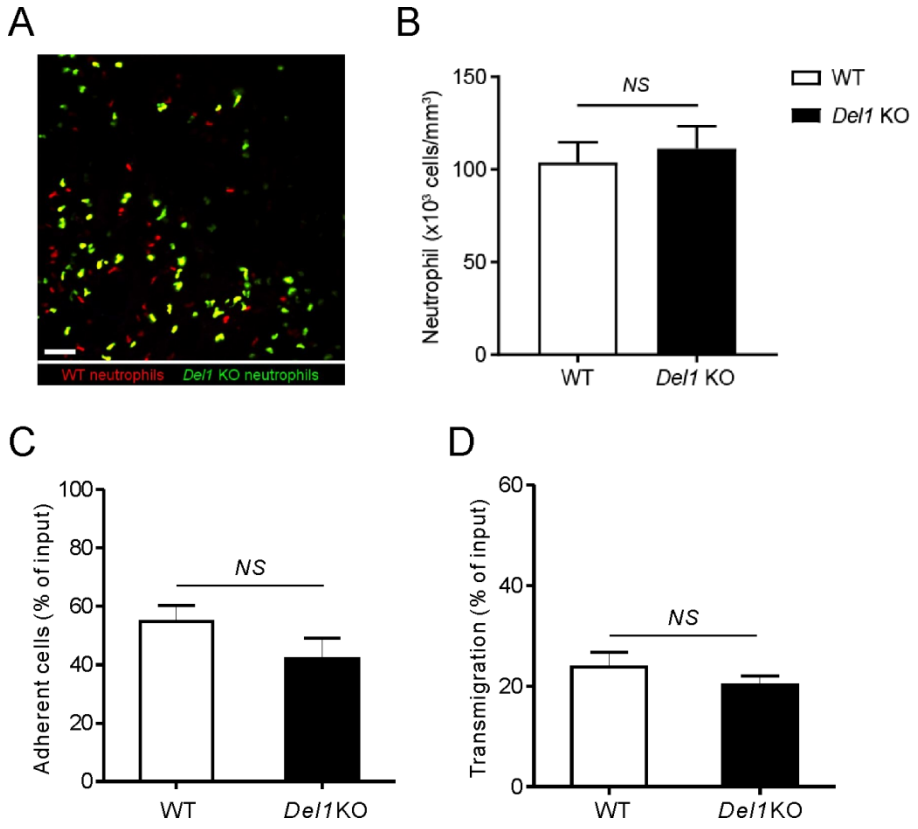

Fig. S13. DEL-1-deficient neutrophils show normal extravasation to the metastasis-bearing lung and adhesion to and transmigration through endothelial cells.

(**A**) Two-photon intravital imaging of WT and *Del1*KO neutrophils recruited to the metastasis-bearing lung of *Del1* KO mice. Neutrophils were isolated from WT and *Del1*KO mice, labeled with CellTracker red CMTPX and CellTracker green CMFDA, respectively, and then i.v. injected at a ratio of 1:1 into *Del1*KO mice 5 days after i.v. inoculation of B16F10 cells. Imaging was performed for 35 min, and representative snapshots were presented (n = 4). Scale bar, 50 µm. (**B**) Quantification of the infiltrating WT and *Del1*KO neutrophils recruited to the metastasis-bearing lung of *Del1* KO mice (n = 4). The number of recruited neutrophils was measured per volume (mm^3). Data are expressed as mean ± SEM. (**C**) Adhesion of WT and *Del1*KO neutrophils onto endothelial cells of *Del1* KO mice is shown. Cell adhesion is presented as the percentage of adherent cells relative to input cells. (**D**) Transmigration of WT and *Del1*KO neutrophils through endothelial cells of *Del1* KO mice is shown in the presence of IL-8 (5 ng/mL). Transmigration is presented as the percentage of input cells. Data are the mean ± SD (n = 5, each group).

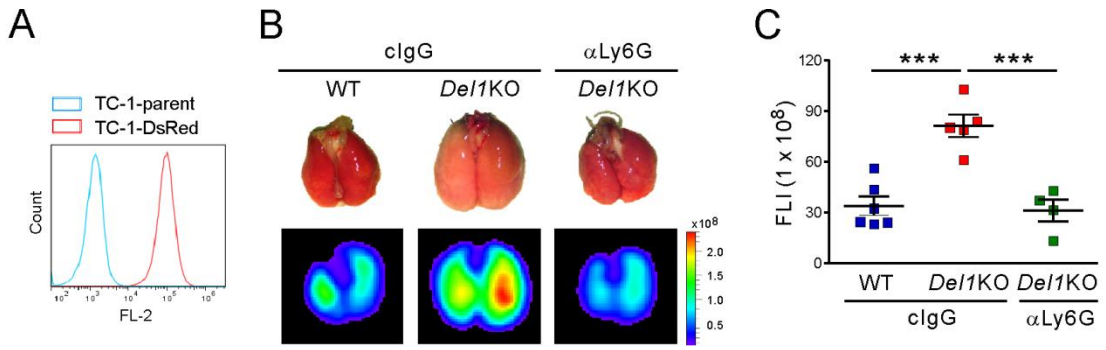

Fig. S14. Pulmonary metastases of TC-1 cells are DEL-1- and neutrophil-dependent. (**A**) Establishment of TC-1 cells expressing DsRed by retroviral transduction. TC-1 cells transduced with DsRed retrovirus were sorted and compared with TC-1 control cells by DsRed expression. (**B**) Representative lung images (top) and the corresponding DsRed fluorescence images (bottom) showing metastases to the lungs of WT (n = 6), *Del1*KO (n = 5), or neutrophil-depleted *Del1*KO (n = 4) mice 2 weeks after i.v. injection of 5×10^5 DsRed-tagged TC-1 cells (day 0). Starting on day -1, *Del1*KO mice received intraperitoneal injections of control IgG or anti-Ly6G antibody and thrice a week treatment thereafter. Photo credit: Hyung-Joon Kwon, University of Ulsan. (**C**) Quantification of lung metastases by FLI depicted in (B). Data are expressed as mean ± SEM. ***P < 0.001.

Supplementary movie legend

Video S1. Intravital imaging of the metastasis-bearing lung after 5 days post-i.v. injection of DsRed-B16F10 cells, related to Fig. 6B.
DsRed-B16F10 melanoma cells (red) and neutrophils (bright green) were identified in the metastasis-bearing lungs of LysM-GFP/WT (left) or LysM-GFP/*Del1* KO mice (right). Scale bar, 50 μm.

Video S2. Migration trajectories of neutrophils in the metastasis-bearing lung of LysM-GFP/WT mice after 5 days post-inoculation of DsRed-B16F10 cells, related to Fig. 6D.
The tracks (white lines) were shown by selected visible neutrophils (green) for 15 min.

Video S3. Migration trajectories of neutrophils in the metastasis-bearing lung of LysM-GFP/*Del1* KO mice after 5 days post-inoculation of DsRed-B16F10 cells, related to Fig. 6D.
The tracks (white lines) were shown by selected visible neutrophils (green) for 15 min.

Video S4. Intravital imaging of WT and *Del1*KO neutrophil infiltration into the metastasis-bearing lung after 5 days post-i.v. injection of B16F10 cells, related to Fig. S13.
WT neutrophils (red) and *Del1*KO neutrophils (green) were identified in the metastasis-bearing lungs of *Del1*KO mice. Scale bar, 50 μm.

Video S5. 3D imaging of the tissue-cleared lung after 5 days post-inoculation of DsRed-B16F10 cells, related to Fig. 6H.
Green, cyan, and red fluorescence represent neutrophils, blood vessels, and B16F10 melanoma cells, respectively.

Video S6. A lung metastatic focus formed after 5 days post-inoculation of DsRed-B16F10 cells was rebuilt into the 3D graphic view, related to Fig. 6, I and J.
For analysis, a single metastatic focus was reconstructed into a graphic mass, and its volume was measured. Neutrophils within 50 μm from the boundaries and inside the metastatic focus were described as green dots, and neutrophils beyond 50 μm from the boundaries of metastatic focus were detected as black dots.